

**POLY(LACTIC ACID) BIONANOCOMPOSITES
REINFORCED WITH TEMPO-OXIDIZED
OIL PALM EMPTY FRUIT BUNCH
NANOCRYSTALLINE CELLULOSE**

ETI INDARTI

UNIVERSITI SAINS MALAYSIA

2017

**POLY(LACTIC ACID) BIONANOCOMPOSITES
REINFORCED WITH TEMPO-OXIDIZED
OIL PALM EMPTY FRUIT BUNCH
NANOCRYSTALLINE CELLULOSE**

by

ETI INDARTI

**Thesis submitted in fulfillment of the requirements
for the degree of
Doctor of Philosophy**

May 2017

ACKNOWLEDGEMENT

Alhamdulillah, I am grateful and thankful to Allah S.W.T, The Great Almighty, for His guidance and blessing until I complete my PhD program. I would like to dedicate my greatest gratitude to my supervisor, Professor Wan Rosli Wan Daud, for his guidance, persistence encouragement, and knowledge sharing throughout this study.

I would like to acknowledge Ministry of Research, Technology, and Higher Education of Indonesia for sponsoring my postgraduate study and Universiti Sains Malaysia for the Research University grant scheme of 1001/PTEKIND/814122 and 1001/PTEKIND/814240. My sincere gratitude to all staff members of the Universiti Sains Malaysia in general and in particular the School of Industrial Technology for their helpful contribution and assistance directly or indirectly.

I would also like to express thank to my beloved husband Dr. Marwan, who give me strength to keep up with study, and my children Muhammad Haikal, Muhammad Qashmal and Muhammad Alfin Khalidi, my parents Ibu Chadijah and Ibu Djauharah for their continuous support and encouragement. A special dedication also goes to all my colleagues and friends who had shared the moment together during my study period. I appreciate all the contribution and this PhD project had given me a lot of knowledge and experience that I believe I could not get elsewhere.

Thank you.

TABLE OF CONTENTS

Acknowledgement.....	ii
Table of Contents.....	iii
List of Tables.....	ix
List of Figures.....	xi
List of Abbreviations.....	xvii
List of Symbols.....	xix
Abstrak.....	xx
Abstract.....	xxii

CHAPTER 1 - INTRODUCTION

1.1 Background.....	1
1.2 Problem Statement.....	3
1.3 Objectives.....	5

CHAPTER 2 – LITERATURE REVIEW

2.1 Cellulose.....	6
2.1.1 Source of Cellulose.....	7
2.1.2 Oil Palm Biomass	7
2.2 Cellulose Molecular Structure.....	10
2.2.1 Supramolecular Structure	11
2.2.2 Morphological Structure	16
2.3 Nanocrystalline Cellulose.....	18
2.3.1 Acid Hydrolysis	20
2.3.2 TEMPO-Oxidation of Cellulose	22
2.3.3 Application of Nanocrystalline Cellulose.....	26

2.4	Modification of Nanocrystalline Cellulose.....	28
2.4.1	Type of Modification	29
2.4.1(a)	Molecular Grafting.....	31
2.4.1(b)	Polymer Grafting.....	33
2.4.2	Silylation.....	35
2.4.3	Mechanism of Silylation.....	37
2.4.3(a)	Hydrolysis.....	39
2.4.3(b)	Adsorption.....	42
2.4.3(c)	Chemically Grafting.....	43
2.5	Polymer Composites.....	43
2.5.1	Bionanocomposites	45
2.5.2	Polylactic Acid.....	47
2.5.2(a)	PLA Structure.....	49
2.5.2(b)	PLA Production.....	50
2.5.2(c)	PLA Properties.....	50
2.5.2(d)	Advantages and Disadvantages of PLA.....	51
2.5.3	Nanocrystalline Cellulose as Reinforcement Agent	53
2.5.3(a)	Interaction between Modified NCC and Polymer Matrix.....	57
2.5.3(b)	Casting of Bionanocomposites.....	58

CHAPTER 3 – MATERIALS AND METHODS

3.1	Materials and Chemicals.....	62
3.2	Pulp Preparation.....	63
3.2.1	Pre-Hydrolysis	63
3.2.2	Soda Pulping.....	64
3.3	Nanocrystalline Cellulose Production.....	64

3.3.1	TEMPO-Mediated Oxidation	65
3.3.2	Post Oxidation with NaClO ₂	65
3.3.3	Nanocrystalline Cellulose Isolation through Sonication	66
3.4	Drying of NCC.....	66
3.4.1	Oven Drying	66
3.4.2	Freeze Drying	67
3.4.3	Solvent Exchange	67
3.5	Redispersing Dried NCC in Chloroform.....	67
3.6	Production of PLA-NCC Bionanocomposite.....	68
3.6.1	Neat PLA Film.....	68
3.6.2	Preparation of Different Concentration NCC Solutions.....	68
3.6.3	Preparation of PLA-NCC Bionanocomposite Film.....	69
3.7	Surface Modification of NCC.....	70
3.8	Preparation of PLA-s-NCC Bionanocomposite Film.....	71
3.9	Characterization Methods.....	72
3.9.1	Nuclear Magnetic Resonance (NMR)	72
3.9.2	Fourier Transform Infrared Spectroscopy (FTIR).....	72
3.9.3	X-Ray Diffraction (XRD) Analysis.....	73
3.9.4	Transmission Electron Microscope (TEM)	73
3.9.5	Scanning Electron Microscope with Energy Dispersive X-Ray (SEM-EDX)	74
3.9.6	Atomic Force Microscope (AFM)	74
3.9.7	Mechanical Properties	75
3.9.8	Differential Scanning Calorimetry (DSC)	76
3.9.9	Thermogravimetric Analysis (TGA)	77
3.9.10	Water Vapor Permeability (WVP)	77
3.9.11	Contact Angle	78

3.9.12 Transparency.....	78
3.9.13 Thickness of Bionanocomposite Film	79

CHAPTER 4 – RESULTS AND DISCUSSIONS

4.1 Nanocrystalline Cellulose Preparation.....	80
4.1.1 FTIR Analysis.....	81
4.1.2 Solid State ¹³ C-NMR Analysis	83
4.1.3 XRD Analysis.....	86
4.1.4 TGA	88
4.1.5 Morphological Observation	90
4.1.6 Dispersion Stability	92
4.1.7 Conclusion	94
4.2 Drying of NCC Suspension	95
4.2.1 FTIR Analysis.....	96
4.2.2 X-ray Diffraction	96
4.2.3 Thermogravimetric Analysis	99
4.2.4 Re-dispersion in Nonpolar Solvent: Chloroform.....	103
4.2.5 Conclusion	106
4.3 Production of PLA-NCC Bionanocomposites using Unmodified OPEFB-NCC.....	107
4.3.1 Morphology	107
4.3.2 ATR- FTIR	109
4.3.3. Thermal Properties of PLA-NCC Bionanocomposites.....	111
4.3.3(a) DSC	111
4.3.3(b) Thermogravimetric Analysis.....	113
4.3.4 Mechanical Properties	115
4.3.5 Water Vapor Permeability	119

4.3.6	Optical Features	122
4.3.7	Conclusion	124
4.4	Chemical Modification of OPEFB-NCC via Silylation Reaction.....	125
4.4.1	Solid State ^{13}C NMR.....	125
4.4.2	Solid-State ^{29}Si NMR.....	129
4.4.3	FTIR.....	131
4.4.4	Morphology	133
4.4.5	XRD	134
4.4.6	Thermal Analysis	136
4.4.7	Wettability of NCC and s-NCC Films.....	137
4.4.8	EDX Analysis of s-NCC.....	139
4.4.9	Dispersion Stability.....	141
4.4.10	Conclusion	143
4.5	Production of PLA-s-NCC Bionanocomposite	145
4.5.1	Morphology	145
4.5.2	ATR-FTIR	147
4.5.3	Thermal Properties.....	149
4.5.3(a)	DSC.....	149
4.5.3(b)	TGA.....	152
4.5.4	Mechanical Properties.....	154
4.5.4(a)	Tensile strength.....	155
4.5.4(b)	Young's Modulus.....	157
4.5.4(c)	Elongation at Break.....	158
4.5.5	Water Vapor Permeability	160
4.5.6	Transparency of PLA-s-NCC Bionanocomposites.....	162
4.5.7	Conclusion	165
4.6	Comparison of PLA- NCC and PLA-s-NCC Bionanocomposites.....	168

4.6.1	SEM Morphology	168
4.6.2	AFM Morphology	170
4.6.3	ATR - FTIR Analysis	172
4.6.4	EDX Analysis	174
4.6.5	Wettability	176
4.6.6	Mechanical Properties.....	179
4.6.7	Thermal Properties.....	182
4.6.8	Water Vapor Permeability	184
4.6.9	Transparency.....	186

CHAPTER 5 – CONCLUSION AND RECOMMENDATION

5.1	Conclusion.....	189
5.2	Recommendation.....	192

REFERENCES.....	193
------------------------	------------

LIST OF PUBLICATIONS

LIST OF TABLES

	Page
Table 2.1 Category of fibers based on their presence in the plants	7
Table 2.2 The difference between TEMPO-oxidized NNC, MFC, and CNC/CNW	20
Table 2.3 Chemical structure and organofunctionality of silane used for natural fiber	36
Table 2.4 Some properties of lactic acid polymer	51
Table 2.5 PLA matrix reinforced with unmodified and modified of cellulose Fiber, MCC, CNF, and NCC	54
Table 3.1 List of chemicals in the experiment.....	62
Table 3.2 NCC concentration in PLA-NCC bionanocomposites forming solution.	69
Table 4.1 FTIR spectral peak assignment for OPEFB pulp and OPEFB NCC	82
Table 4.2 Thermal properties of OPEFB-pulp and OPEFB-NCC.....	89
Table 4.3 Intensity peak of FTIR spectra	97
Table 4.4 Crystallinity Index (CI) of OPEFB pulp and NCC	98
Table 4.5 Thermal properties of OPEFB pulp, OD-NCC, FD-NCC, and SE-NCC	102
Table 4.6 Thermal properties and crystallinity of PLA-NCC bionanocomposites	112
Table 4.7 Thermal properties of NCC, neat PLA, and PLA-NCC bionanocomposites	115
Table 4.8 Mechanical properties of neat PLA and PLA-NCC bionanocomposites	117
Table 4.9 WVP for PLA and PLA-NCC bionanocomposites	120
Table 4.10 List of signals and integrity of C atom chain of NCC and s-NCC...	126
Table 4.11 FTIR spectral peak assignment for (a) NCC and (b) s-NCC.....	132
Table 4.12 The geometrical dimensions of NCC and s-NCC.	134
Table 4.13 Quantification of the spatial element distribution obtained by SEM–EDX for NCC and s-NCC.....	140

Table 4.14	Thermal properties and crystallinity of the neat PLA and PLA-s-NCC	150
	Table 4.15 Thermal properties of s-NCC, neat PLA, and PLA-s-NCC	153
Table 4.16	The mechanical properties of neat PLA and PLA-s-NCC.	155
Table 4.17	Comparison result of tensile strength at break.	156
Table 4.18	The mechanical properties of neat PLA film derive from different PLA sources.....	160
Table 4.19	WVP reduction of PLA-s-NCC bionanocomposite at different filler loading.....	161
Table 4.20	Atomic composition from EDX for PLA-NCC and PLA-s-NCC.	175
Table 4.21	DSC parameters determined from the first heating scan.....	182
Table 4.22	Barrier behavior of neat PLA, PLA-NCC, and PLA-s-NCC.	185
Table 4.23	Percentage of light transmission at visible region for the PLA bio-nanocomposites at different filler loadings.	188

LIST OF FIGURES

	Page
Figure 2.1 Sketch of (a) oil palm fruit bunch (b) cross section of oil palm fruit bunch showing fiber arrangement	8
Figure 2.2 View of EFB wastes piled up in a palm oil mill premise	8
Figure 2.3 Growth of different biomass wastes from oil palm industries	9
Figure 2.4 Chemical composition of oil palm biomass	10
Figure 2.5 Structure of cellulose	11
Figure 2.6 Main steps to produce polymorphs of cellulose	12
Figure 2.7 Schematic of the unit cells for cellulose I _α (triclinic) and I _β (monoclinic)	13
Figure 2.8 Molecule chain direction of (a) cellulose I parallel and (b) cellulose II anti-parallel structure	14
Figure 2.9 Supramolecular distinction between (a) cellulose I and (b) cellulose II lies in inter and intramolecular hydrogen bonds	15
Figure 2.10 Schematics illustration of cellulose microfibril showing one of the suggested configurations of the crystalline and amorphous regions.....	16
Figure 2.11 From the cellulose source to the cellulose molecules:	17
Figure 2.12 Schematic illustration for the isolation of the crystalline structure of cellulose by acid hydrolysis	21
Figure 2.13 Mechanism of regioselective oxidation of cellulose by TEMPO-mediated oxidation	23
Figure 2.14 Illustration for the oxidation of C6 primary hydroxyls on native cellulose microfibril surfaces to C6 carboxylate groups using the TEMPO system	23
Figure 2.15 Schematic diagram of cellulose degradation by ultrasonic process.	25
Figure 2.16 Modification chemistries of CN surfaces	29
Figure 2.17 Methods for preparation of graft copolymers on the nanocellulose surface: (a) “grafting onto”, (b) “grafting from”	34
Figure 2.18 Molecular structure of 3-aminopropyltriethoxysilane.....	36

Figure 2.19	Mechanism of silylation onto the cellulose surface	38
Figure 2.20	Different length of bridge connecting the silicon atom and functionalities for (a) α -silane with a methylene spacer, (b) γ -silane with a propylene spacer, and (c) “ α -effect” in the aminomethylene silane	40
Figure 2.21	A proposed cyclic hydrogen-bonded amine structure in the hydrolytic APS solution.....	41
Figure 2.22	Classification of Plastic based on source and degradation properties	44
Figure 2.23	Classification of polymer matrix applicable to cellulose based nanocomposites	46
Figure 2.24	PLA production among bioplastic production prediction in 2017	48
Figure 2.25	Global PLA market by application at period of 2012 – 2020	48
Figure 2.26	Chemical structure of (a) L-lactic acid and D-lactic acid, and (b) polylactic acid	49
Figure 3.1	Experimental outline	61
Figure 3.2	Solvent casting of PLA-nanocomposites.....	68
Figure 3.3	Apparatus for modification NCC	70
Figure 3.4	Schematic observation of contact angle	78
Figure 4.1	FTIR spectra of (a) OPEFB-pulp and (b) OPEFB-NCC	81
Figure 4.2	CP/MAS ^{13}C -NMR spectrum of (a) OPEFB-Pulp, and (b) OPEFB-NCC.	84
Figure 4.3	Schematic drawing of TEMPO reaction of a cellulose chain on the surface of a cellulose crystal	85
Figure 4.4	X-ray diffraction of (a) OPEFB-pulp and (b) TEMPO-oxidized OPEFB-NCC.....	86
Figure 4.5	TGA profile of (a) OPEFB pulp and (b) OPEFB NCC.....	88
Figure 4.6	DTG profile of (a) OPEFB-pulp and (b) OPEFB-NCC	88
Figure 4.7	Visual appearance of the cellulose sample. (a) Raw OPEFB, (b) OPEFB pulp, (c) TEMPO-oxidized pulp, and (d) post TEMPO oxidized pulp.	90
Figure 4.8	SEM image of bundle (a) and single (b) OPEFB-pulp fiber	91
Figure 4.9	TEM images of (a) OPEFB-pulp, and (b) OPEFB-NCC	92

Figure 4.10	Comparison of pulp (left) and NCC (right) suspension in water stood for (a) 0 minute, (b) 5 minute, and (c) 15 minute.	93
Figure 4.11	Birefringent of NCC suspension in water	93
Figure 4.12	Typical FTIR spectra obtained from (a) OPEFB pulp, (b) OD-NCC, (c) FD-NCC and (d) SE-NCC	96
Figure 4.13	X-ray diffractograms from (a) OPEFB pulp, (b) FD-NCC, (c) OD-NCC, and (d) SE-NCC.....	98
Figure 4.14	TGA profiles of FD-NCC, SE-NCC, OD-NCC, and OPEFB pulp.....	100
Figure 4.15	DTG profiles of FD-NCC, SE-NCC, OD-NCC, and OPEFB pulp.....	100
Figure 4.16	NCC suspension prior to water separation (a), and suspension after 15 min of re-dispersion in chloroform for (b) OD-NCC, (c) SE- NCC, and (d) FD-NCC.	104
Figure 4.17	(a) TEM of redispersed OPEFB-NCC in chloroform and (b) SEM of PLA-OPEFB NCC bionanocomposite with 5% OPEFB-NCC.....	107
Figure 4.18	SEM images of fracture surfaces for (a) neat PLA, (b) PLA-NCC1, (c) PLA-NCC3, (d) PLA-NCC5, (e) PLA-NCC10, and (f) PLA-NCC20 bionanocomposites at 2000 x magnification.	109
Figure 4.19	ATR-FTIR spectra of (a) NCC, (b) neat PLA, and bionanocomposite films (c) PLA-NCC1, (d) PLA-NCC3, (e) PLA-NCC5, (f) PLA-NCC10, and (g) PLA-NCC20.....	110
Figure 4.20	DSC thermograms for heating scans of (a) neat PLA, (b) PLA-NCC1, (c) PLA-NCC3, (d) PLA-NCC5, (e) PLA-NCC10, and (f) PLA-NCC20.....	111
Figure 4.21	TGA profiles of NCC, neat PLA, and PLA-NCC bionanocomposites.	114
Figure 4.22	DTG profiles of NCC, neat PLA, and PLA-NCC bionanocomposites.	114
Figure 4.23	Effect of NCC concentration on PLA matrix on (a) tensile strength, and (b) elongation, and (c) Young's Modulus.....	116
Figure 4.24	Visual comparison of the transparency of (a) neat PLA, (b) PLA-NCC1, (c) PLA-NCC3, (d) PLA-NCC5, (e) PLA-NCC10, and (f) PLA-NCC20.....	122

Figure 4.25	Light transmittance of neat PLA and PLA-NCC bionanocomposites at different wavelengths.....	123
Figure 4.26	Solid State ^{13}C NMR spectra of (a) NCC and (b) s-NCC	126
Figure 4.27	Proposed reaction between functional groups of the cellulose and the 3-aminopropyltriethoxysilane.....	127
Figure 4.28	Description of signal position of APS fragments.	128
Figure 4.29	Solid State ^{29}Si CP/MAS NMR spectra of s-NCC.	129
Figure 4.30	The identification Si chemical structure in the form of (a) T1, (b) T2, and (c) T3. (R alkyl group from cellulose, R' alkyl group bond to organofunctionality (NH_2)	130
Figure 4.31	Structural possibility anticipated for APS derivatized on the NCC surface.	130
Figure 4.32	FTIR spectra of (a) NCC and (b) s-NCC.....	131
Figure 4.33	TEM images of (a) NCC and (b) s-NCC.....	134
Figure 4.34	XRD pattern of (a) NCC and (b) s-NCC.	135
Figure 4.35	TGA profile of (a) NCC and (b) s-NCC.....	136
Figure 4.36	DTG profile of (a) NCC and (b) s-NCC.....	137
Figure 4.37	Photographs of water droplet over thin film made of (a) NCC and (b) s-NCC.....	138
Figure 4.38	Contact angle of water droplet over thin film made of (a) NCC and (b) s-NCC.....	138
Figure 4.39	EDX spectra and its elemental identification of (a) NCC and (b) s-NCC.....	140
Figure 4.40	SEM-EDX images of the s-NCC; (a) image, (b) X-ray count for Si, and (c) X-ray count for N.	141
Figure 4.41	Redispersed NCC in (1) chloroform and (2) s-NCC in chloroform at (a) day 0, (b) day 1, and (c) day 2.	142
Figure 4.42	SEM images of cryo-fracture surface of the PLA-s-NCC bionanocomposite at (a) neat PLA, (b) PLA-s-NCC1, (c) PLA-s-NCC3, (d) PLA-s-NCC5, (e) PLA-s-NCC10 and (f) PLA-s-NCC20.	146
Figure 4.43	ATR-FTIR spectra of (a) s-NCC, (b) neat PLA, and bionanocomposite films of (c) PLA-s-NCC1, (d) PLA-s-NCC3, (e) PLA-s-NCC5, (f) PLA-s-NCC10, and (g) PLA-s-NCC20	147

Figure 4.44	The proposed reaction mechanism between s-NCC and PLA matrix	148
Figure 4.45	DSC profile of (a) neat PLA, and bionanocomposite films (b) PLA-s-NCC1, (c) PLA-s-NCC3, (d) PLA-s-NCC5, (e) PLA-s-NCC10, and (f) PLA-s-NCC20.	149
Figure 4.46	TGA profile of PLA-s-NCC bionanocomposites	152
Figure 4.47	DTG profile of PLA-s-NCC bionanocomposites	153
Figure 4.48	Effect of s-NCC concentration on tensile strength of PLA-s-NCC.	155
Figure 4.49	Young's Modulus of neat PLA and PLA-s-NCC.....	158
Figure 4.50	The elongation at break of neat PLA and PLA-s-NCC.....	159
Figure 4.51	WVP profile of the PLA-s-NCC bionanocomposite at different filler loadings.	161
Figure 4.52	The transparency of (a) neat PLA (b) PLA-s-NCC1, (c) PLA-s-NCC3, (d) PLA-s-NCC5, (e) PLA-s-NCC10, (f) PLA-s-NCC20.	163
Figure 4.53	Optical characterization of neat PLA and PLA-s-NCC	164
Figure 4.54	SEM images of fracture surfaces for PLA with unmodified (PLA-NCC) and Modified NCC (PLA-s-NCC); (a), PLA-NCC5 (b), PLA-s-NCC5, (c) PLA-NCC10, (d) PLA-NCC10, at 2000 x magnification.	168
Figure 4.55	Surface of (a) NCC and (b) s-NCC in the PLA matrix at a higher magnification.	169
Figure 4.56	Typical atomic force microscope images of (a) neat PLA, (b) PLA-NCC10, and (c) PLA-s-NCC10.	171
Figure 4.57	ATR-FTIR spectra of (a) neat PLA, (b) PLA-NCC, and (c) PLA-s-NCC.....	172
Figure 4.58	EDX spectra of PLA-NCC and PLA-s-NCC.	174
Figure 4.59	EDX images of PLA-s-NCC.	175
Figure 4.60	Shape of water droplet on surface of (a) neat PLA, (b) PLA-NCC10, and (c) PLA-s-NCC10.	177
Figure 4.61	Degree of contact angle of (a) neat PLA, (b) PLA-NCC10, and (c) PLA-s-NCC10.....	177
Figure 4.62	Tensile properties of neat PLA, PLA-NCC, and PLA-s-NCC.....	179

Figure 4.63	Young's modulus of PLA NCC and PLA-s-NCC.	180
Figure 4.64	Elongation at break of PLA-NCC and PLA-s-NCC.	181
Figure 4.65	Visual image (a) without film and with films of (b) neat PLA, (c) PLA-NCC10, (d) PLA-s-NCC10, (e) PLA-NCC20, and (f) PLA-s-NCC20.....	187
Figure 4.66	Light transmission at visible region (wavelength 550 nm) for the PLA bionanocomposites at different filler loadings.....	188

LIST OF ABBREVIATIONS

4-AcNH-TEMPO	4-acetamido-TEMPO
AFM	Atomic Force Microscope
APS	Aminopropyltriethoxysilane
ATR	Attenuated Total Reflectance
COO ⁻	Carboxylate anion
COOH	Protonate carboxylic acid
DSC	Differential Scanning Calorimeter
DTG	Derivative Thermogravimetry
EDX	Energy Dispersive X-Ray Spectroscopy
FTIR	Fourier Transform Infrared Spectroscopy
OD-NCC	Oven dried nanocrystalline cellulose
FD-NCC	Freeze dried nanocrystalline cellulose
SE-NCC	Solvent exchanged nanocrystalline cellulose
NCC	Nanocrystalline cellulose
s-NCC	Silylated NCC
NMR	Nuclear Magnetic Resonance
OPEFB	Oil palm empty fruit bunch
OPEFB-NCC	Oil palm empty fruit bunch nanocrystalline cellulose
OPEFB-Pulp	Oil palm empty fruit bunch pulp
PLA	Polylactic acid
PLA-NCC	Polylactic acid – nanocrystalline cellulose
PLA-s-NCC	Polylactic acid – silylated nanocrystalline cellulose
RH	Relative humidity
SEM	Scanning Electron Microscopy

T _c	Crystallization temperature
T _g	Glass transition temperature
T _m	Melting temperature
TEM	Transmission Electron Microscopy
TEMPO	2,2,6,6,-tetramethyl-1-piperidinyloxy
TGA	Thermogravimetric Analysis
UV-Vis	Ultra Violet Visible
WVP	Water Vapor Permeability
XRD	X-ray Diffraction

LIST OF SYMBOLS

%	Percentage
w/w	Weight per weight
w/v	Weight per volume
°C	Degree Celsius
psi	Pound per square inch
rpm	Revolutions per minute
L	Liter
Hz	Hertz
N	Newton
g	Gram
MPa	Mega Pascal
GPa	Giga pascal
s	Second
ppm	Parts per million
h	Hour
k	Kilo
M	Mega
n	Nano
μ	Micro
X _c	Degree of crystallinity
ΔH _m	Enthalpy at melting stage

BIONANOKOMPOSIT POLI(LAKTIK ASID) DIPERKUAT DENGAN SELULOSA NANOKRISTAL TANDAN BUAH KELAPA SAWIT KOSONG TEMPO-TEROKSIDA

ABSTRAK

Bionanokomposit poli(laktik asid) (PLA) dan selulosa nanokristal (NCC) mempunyai potensi untuk digunakan dalam pelbagai aplikasi kerana ianya terbiodegradasi dan boleh diperbaharui. Walau bagaimanapun, kerana perbezaannya yang ketara dalam kebolehan hidrofobik, ia membentuk masalah penyerakan dan keserasian. Untuk mengurangkan kelemahan-kelemahan ini, NCC ini diubahsuai melalui tindak balas sililasi menggunakan 3-aminopropiltrietoksisilana (APS). NCC yang digunakan dalam kajian ini telah diasingkan daripada pulpa takterluntur OPEFB menggunakan kombinasi pengoksidaan TEMPO dan rawatan ultrasonik, dengan penuangan pelarut menggunakan klorofom digunakan bagi penyediaan bionanokomposit PLA-NCC. Pencirian-pencirian bahan telah dilakukan menggunakan pelbagai analisis seperti SEM, TEM, FTIR, ^{13}C dan ^{29}Si NMR keadaan pepejal. Bagi bionanokomposit, sebagai tambahan bagi analisis-analisis ini, mereka juga dikenakan kepada DSC, TGA, mekanikal, kebolehan telapan air, AFM dan ujian kebasahan. Pengesanan bagi TEMPO teroksida NCC diperoleh melalui puncak baru FTIR pada 1732 cm^{-1} dan isyarat baru NMR pada 174 ppm. Gambar TEM bagi NCC mempamirkan seperti rod kristal dengan purata lebar 5.0 nm dan nisbah axial 45. Bukti bagi kejayaan sililasi menggunakan 3-aminopropiltrietoksisilana (APS) dapat dilihat daripada munculnya puncak baru FTIR pada 749, 1505, dan 2928 cm^{-1} , isyarat baru ^{13}C NMR pada 42.7, 21.7 dan 10.3 ppm, dan puncak baru ^{29}Si NMR pada -69, -61 dan -43 ppm, dan daripada analisis EDX mendapati kehadiran penyerakan yang bagus bagi

elemen Si di dalam NCC. Padanan bagi sililasi NCC (s-NCC) ke dalam matrik PLA mempunyai kesan yang memberangsangkan bagi sifat-sifat bionanokomposit tersebut. Penambahan bagi 1-10brt% bagi s-NCC di dalam PLA menghasilkan peningkatan sehingga 33.3% dan 47.0% masing-masing bagi kedua-dua kekuatan tegangan dan modulus Young jika dibandingkan dengan NCC. Walau bagaimanapun, pemanjangan ketika putus berkurang sehingga 57% dengan penambahan s-NCC. Kestabilan terma yang ditentukan dari baki di dalam analisis TGA adalah lebih tinggi dari PLA-NCC. Pemerhatian visual dan spektroskopi UV-Vis tidak menunjukkan apa-apa penurunan yang signifikan dalam transmisi cahaya walaupun pada penambahan 20%. Sifat penghalang air bagi PLA-s-NCC seperti yang diukur melalui WVP, memberikan peningkatan sebanyak 27% dengan penambahan s-NCC. AFM dan EDX analisis kedua-duanya menunjukkan serakan yang lebih baik bagi s-NCC di dalam matrik PLA. Apabila membandingkan kedua-dua jenis PLA bionanokomposit, ia jelas kelihatan bahawa PLA-s-NCC mempunyai prestasi yang lebih baik dari segi kekuatan, kestabilan terma, keupayaan halangan air dan sifat optik. Menjadi terbiodegradasikan, dan memandangkan s-NCC boleh ditambah sehingga 20% tanpa mengurangkan apa-apa sifat secara signifikan, pengisi nano bagi TEMPO-NCC tersililasi ini mempunyai potensi untuk menjanjikan calon pilihan untuk pelbagai aplikasi.

**POLY(LACTIC ACID) BIONANOCOMPOSITES REINFORCED WITH
TEMPO-OXIDIZED OIL PALM EMPTY FRUIT BUNCH
NANOCRYSTALLINE CELLULOSE**

ABSTRACT

Bionanocomposites of poly(lactic acid) (PLA) and nanocrystalline cellulose (NCC) have the potentials to be used in various applications because of their biodegradability and renewability. However, due to their significant differences in hydrophobicity, it creates dispersibility and compatibility problems. To reduce these shortcomings, the NCC is modified via the silylation reaction using 3-aminopropyltriethoxysilane (APS). The NCC used in this research was isolated from unbleached OPEFB pulp using a combination of TEMPO oxidation and ultrasonic treatment, with solvent casting using chloroform employed for the preparation of the PLA-NCC bionanocomposite. Material characterizations were carried out using various analysis such as SEM, TEM, FTIR, ^{13}C and ^{29}Si Solid State NMR. For the bionanocomposites, in addition to these analysis, they were also subjected to DSC, TGA, mechanical, water vapour permeability, AFM and wettability tests. Confirmation of the TEMPO oxidized NCC was obtained through a new FTIR peak at 1732 cm^{-1} and a new NMR signal at 174 ppm. TEM image of the NCC exhibits rod like crystals with the average width of 5.0 nm and axial ratio of 45. Evidence of a successful silylation using 3-aminopropyltriethoxysilane (APS) can be seen from the emergence of new FTIR peaks at 749, 1505, and 2928 cm^{-1} , new ^{13}C NMR signals at 42.7, 21.7 and 10.3 ppm, and new ^{29}Si NMR peaks at -69, -61 and -43 ppm, and from EDX analysis it indicates the presence of well dispersed Si element in the NCC. Incorporation of the silylated NCC (s-NCC) into the PLA matrix have a remarkable

effect on their bionanocomposite properties. An addition of 1-10 wt% of s-NCC in PLA resulted in increment of up to 33.3% and 47.0% respectively in both tensile strength and Young's modulus as compared to NCC. However, elongation at break decreases up to 57% with increase in s-NCC. Thermal stability as determined from the residue in the TGA analysis is higher than the PLA-NCC. Visual and UV-Vis spectroscopic evaluation do not show any significant reduction in light transmission even at 20% addition. Water barrier property of the PLA-s-NCC as measured by WVP, confers an increase of 27% with increase in the s-NCC loading. Both of AFM and EDX analysis show better dispersion of the s-NCC in the PLA matrix. Upon comparing both types of PLA bionanocomposites, it is obvious that the PLA-s-NCC has a much better performance in terms of strength, thermal stability, water barrier capability and optical property. Being biodegradable, and considering s-NCC can be added up to 20% without significantly impairing any property, this nanofiller of silylated TEMPO-NCC has the potentials to be a promising candidate for various applications.

CHAPTER 1

INTRODUCTION

1.1 Background

Poly(lactic acid) (PLA), is currently one of the largest produced bio-based polymer worldwide with a forecasted production of around one million tonnes by 2020 (Grand-View-Research, 2015) and also amongst the most highly researched biopolymer (Lasprilla et al., 2012) which has been used and has have the potentials for various end-use applications. PLA is well known for its renewability, biodegradability, and excellent transparency (Frone et al., 2013), however it also suffers some serious drawbacks such as low thermal resistance, brittleness, and water vapor permeability (Fortunati et al., 2012b). To ameliorate these shortcomings, several different strategies have been adopted, amongst which are modification of the PLA matrix itself (Sin et al., 2012), blending with other polymers such as LDPE (Hamad et al., 2012), use of reinforcing agents such as glass fibers (Lin et al., 2015), nanoclays (Kaiser et al., 2013), carbon nanotubes (Akbari et al., 2015) and cellulosic fibers (Baheti et al., 2013), of which the latter have been extensively studied in view of enhancing the PLA properties (Cheng et al., 2011) due to their unique properties, such as its non-toxicity, swelling ability and stability under variations in temperature and pH. Since the PLA and cellulosic materials are both biodegradable and bio-based, the product of such composite material is aptly called biocomposite.

Cellulosic fibers can be extracted from both woody and non-woody sources with oil palm biomass being the most prospective in the Southeast Asia region, particularly Malaysia and Indonesia. These residues represent an abundant, inexpensive, and readily available source of cellulose from a renewable biomass.

Malaysia has enormous quantities of this lignocellulosic material which comprises of oil empty fruit bunches (OPEFB), fibers, shells, wet shells, palm kernels, fronds and trunks, with OPEFB being the most potential because of its high alpha cellulose content of 42.7 - 65%, and availability of around 7 million tonnes in 2015 (Law et al., 2007; Shinoj et al., 2011; Wanrosli et al., 2004).

Among the various types of cellulosic materials such as pulp, microcrystalline cellulose (MCC), and nanocrystalline cellulose (NCC), with the latter generating considerable interest because of its potential to improve mechanical and barrier properties of PLA biocomposites; these effects are related to the high specific area and Young's modulus (145 to 150 GPa) of NCC (Miao & Hamad, 2013). The composite comprising of NCC and PLA is acknowledged as bionanocomposite since the dimension of the NCC are in nanometer range (Mariano et al., 2014).

NCC is usually isolated from the crystalline regions of cellulose fibers via strong acid hydrolysis, mainly using sulfuric acid at elevated temperatures (Abraham et al., 2011; Al-Dulaimi & Wanrosli, 2016; Dufresne, 2013; Goh et al., 2016). This method produces surface negative charges by way of the sulphate groups that are induced during the reactions which will help to improve the dispersibility wherein aggregation is prevented by the electrostatic repulsion between the particles. Apart from being in a corrosive system, another disadvantage of the acid hydrolysis is its relatively low yield of 30-50% (Isogai et al., 2011; Börjesson & Westman, 2015). Recently, NCC has been prepared from OPEFB cellulose using 2,2,6,6-tetramethylpiperidine-1-oxy (TEMPO) mediated oxidation, followed by mechanical disintegration of ultrasonification (Rohaizu & Wanrosli, 2017). The TEMPO radical helps to introduce additional carboxylic groups onto the fibers, thus allowing them to form dispersions of individualized fibers in water. In addition to the induction of a

negatively charged surface, the TEMPO-oxidation method is also advantageous due to its capability to produce oxidized yields of up to 90% (Rohaizu & Wanrosli, 2017; Saito et al., 2007).

1.2 Problem Statement

Preparation of PLA based bionanocomposites reinforced by NCC by solvent casting is of interest in this research. Advantages of the solvent casting method include the possibility of obtaining uniform thickness distribution, maximum optical purity and extremely low haze (Bonilla et al., 2013). It also gives opportunity of production of high-temperature resistant films from non-melting but soluble raw materials. The process does not require energy extensively. In practice, solvent casting prefers use of non-polar media such as chloroform to allow quick evaporation during film standing.

PLA is readily dissolved in chloroform, however NCC is not well dispersed in chloroform due to the electrostatic character of the suspension stability. Therefore, the preparation of a stable dispersion of the NCC prior to mixing with the PLA solution is crucial in order to obtain a good interaction between NCC and PLA. NCC that is prepared from the TEMPO oxidation process is in the form of an aqueous solution, hence the challenge is to produce a dried form of NCC that can dispersed in chloroform before mixing with the PLA in a polar solution of chloroform. This is important since it determines the extent of the NCC dispersibility in the PLA matrix, which will have an affect on the properties of the final bionanocomposite. Various ways such as solvent exchange, freeze drying and oven drying has been proposed (Fujisawa et al., 2013; Peng et al., 2013), the latter is of particular interest because of its relatively straightforward and inexpensive process. Nevertheless, due to the strong preference of hydrogen bonding among the cellulose chains when in close proximity with each

other, one of the biggest encumbrances at this stage is to minimize the agglomeration of the NCC's. This research will attempt to reduce this problem via a modified oven drying process. In addition, another problem which is inherent with NCC that limits its use is the incompatibility with most polymeric matrices such as PLA. Principally this is due to their character differences whereby NCC is a hydrophilic material and PLA a hydrophobic one; this reduces their interfacial interaction resulting in adverse properties on the final bionanocomposite. To overcome this drawback, it necessitates chemical modifications, with several strategies being adopted, such as adsorbed surfactant (Habibi, 2014), graft polymerization (Fujisawa et al., 2013), and silane treatment (Rachini et al., 2012).

Although the incorporation of oil palm based cellulose into PLA has been investigated (Baheti et al., 2013; Fortunati et al., 2015; Frone et al., 2016), the use of TEMPO oxidized OPEFB-NCC has never been reported before. This is particularly interesting because of the presence of carboxylic groups in the NCC which could possibly modify its surface chemistry, and in doing so could enhance the compatibility of the NCC with PLA.

The research conducted in this thesis will utilize NCC that is isolated from OPEFB via the TEMPO oxidation process to enhance the properties of the PLA bionanocomposites. It will address the issues of poor dispersibility and compatibility of NCC and the PLA through the development of a modified oven dried process for the purpose of removing water from the NCC suspension and modification of the NCC via silylation reaction, both of which are expected to lead to an improved PLA-NCC bionanocomposite properties.

1.3 Objectives

The objectives of this research is to produce poly(lactic acid) bionanocomposites filled with nanocrystalline cellulose (NCC) from TEMPO-oxidized oil palm biomass. To fulfill this aim, the following objectives will be carried out:

- a) To isolate NCC from OPEFB using the TEMPO oxidation method
- b) To produce dried NCC using a modified oven drying process.
- c) To produce PLA-unmodified NCC bionanocomposites.
- d) To modify NCC using 3-aminopropyl triethoxysilane (APS).
- e) To produce PLA-modified NCC bionanocomposites.

CHAPTER 2

LITERATURE REVIEW

2.1 Cellulose

Cellulose is the most abundant biopolymer on earth, and is naturally available as fibers in wood, bushes, cotton, and bast plants, as well as other living species such as plants, animals, and some bacteria (Kalia et al., 2014) with estimated annual production of 1.5 trillion tons and considered as an almost inexhaustible source of raw materials. Of this, only about 6 billion tons are processed by industries such as paper, textile, material and chemical industries (Ball, 2005; Kim et al., 2015). Therefore, the dominant pathway to produce cellulose is from plants. The main substance of cell wall in lignocellulosic plants is cellulose, and its content varies depending on the species, growth, position, growing environment, and maturity. In the cotton seed hairs, the cellulose is found in almost pure form. On the other hand, wood cellulose builds native composite materials of the plants with hemicelluloses and lignin. Nowadays, wood remains the main source of cellulose which is produced in a large-scale mainly through the sequential processes of chemical pulping, separation, and purification.

The fascination of the cellulose biopolymer comes from its specific structure. The combination of both carbohydrate and polymer chemistry consisted of repeating glucose units constructs cellulose macromolecules with amazing specificity and impressively diverse architectures, functions and reactivities (Klemm et al., 2005). Irrespective of its source, cellulose is white fiber-like crystals and odorless. However, fibers of various origins have different shape and dimensions. Cotton fibers are long enough within a range of centimeters lengths, while fibers of wood are typically short, 1-3 mm in length.

2.1.1 Source of Cellulose

Although the cellulose is primarily originated from wood, there are other non-woody sources of fibers such as cotton, jute, flax, bacteria, marine animals (tunicate), invertebrates, algae, and fungi. Cellulose source can also be categorized according to their position in the plant as given in Table 2.1.

Table 2.1 Category of fibers based on their presence in the plants

Category	Description	Examples	Cellulose Content (%)
Stalk fibers	Fibers are actually the stalks of the plant	Rice, barley, wheat straws, bamboo, grass, tree wood	40-50
Fruit fibers	Fibers are collected from the fruit of the plant	Coconut fiber, oil palm fruitbunch	30-50
Bast fibers	Fibers are collected from the skin or bast surrounding the stem of their respective plants	Flax, jute, kenaf, hemp, ramie, rattan, vine fibers	33
Seed fibers	Fibers collected from seeds or seed cases	Cotton, kapok	90
Leaf fibers	Fibers collected from leaves	Sisal, fique, agave	33

Source: (Lavanya et al., 2011)

2.1.2 Oil Palm Biomass

Considerable efforts have been directed towards utilization of biomass waste, for instances oil palm wastes (Rohaizu & Wanrosli, 2017; Rosli et al., 2003b), pea hulls (Fleming et al., 2001a), bagasse (Mandal & Chakrabarty, 2011), and rice straw (Jiang & Hsieh, 2013). Oil palm biomass (OPB) becomes one of the most prominent sources of cellulose for the south-east Asian countries. OPB is a solid waste by-product

that resulted from the oil palm industry, available in several forms such as empty fruit bunches (Figure 2.1), fiber, shell, palm kernel, fronds, and trunk. Around 75% of the wastes in the form of trunks and frond are left decomposed in the plantation for mulching and nutrient replacement, while the remaining 25% biomass such as palm kernel shell, empty fruit bunch, and mesocarp fiber are utilized in the power plant (Awalludin et al., 2015). These residues represent an abundant, inexpensive, and readily available lignocellulosic source of renewable biomass (Wanrosli et al., 2011).

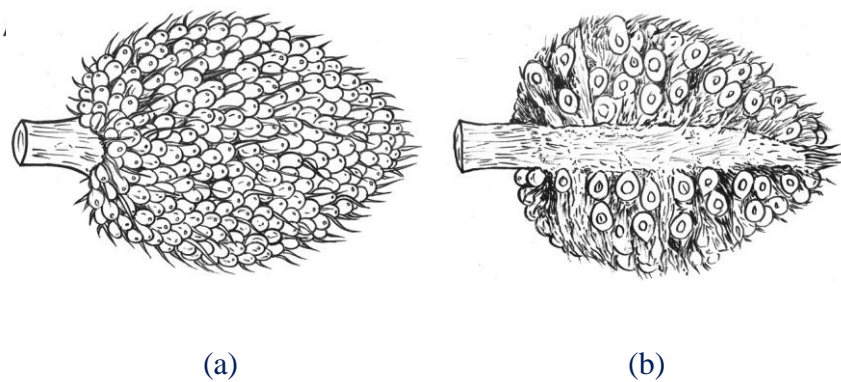


Figure 2.1 Sketch of (a) oil palm fruit bunch (b) cross section of oil palm fruit bunch showing fiber arrangement (Shinoj et al., 2011)



Figure 2.2 View of EFB wastes piled up in a palm oil mill premise (Shinoj et al., 2011)

In 2015, Malaysia is estimated to produce 85-95 million tons of OPB (Agensi Inovasi Malaysia, 2013), thus making these lignocellulosic wastes a major disposal problem (Figure 2.2) and palm oil industry dump about 1.1 ton of EFB for each ton of oil produced (Karina et al., 2008). On the other hand, OPB utilization does not compete its food production (Abdullah & Sulaiman, 2013). It has been noted that the high cellulose content about 60.6% in EFB hence the highest yield of fiber up to 73% compared to other fiber sources in an oil palm tree (Wanrosli et al., 2004) indicate an enormous potential to be exploited for high value cellulose, particularly in the form of nanocellulose crystalline (NCC). Figures 2.3 and 2.4 show the estimated growth and chemical composition, respectively, of each biomass type collected in the oil palm plantation in Malaysia.

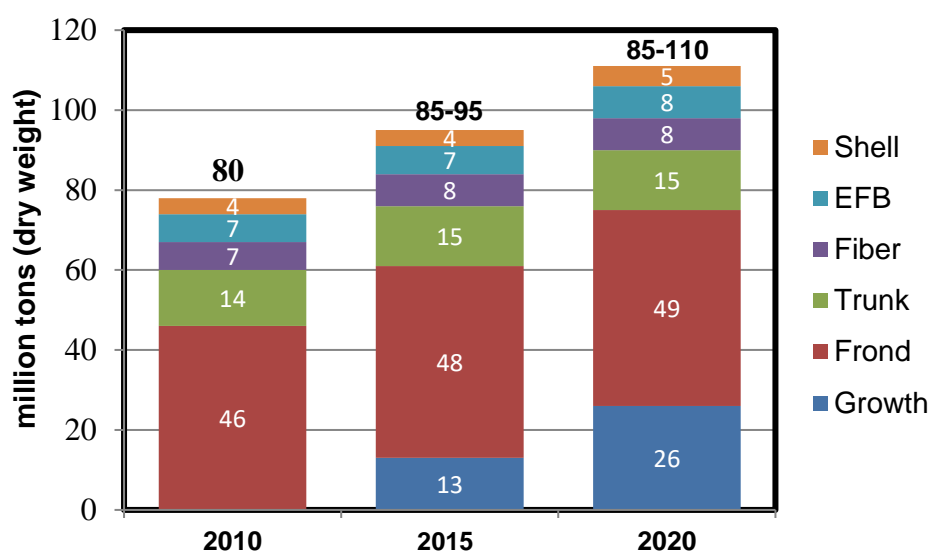


Figure 2.3 Growth of different biomass wastes from oil palm industries (Agensi-Inovasi-Malaysia, 2013)

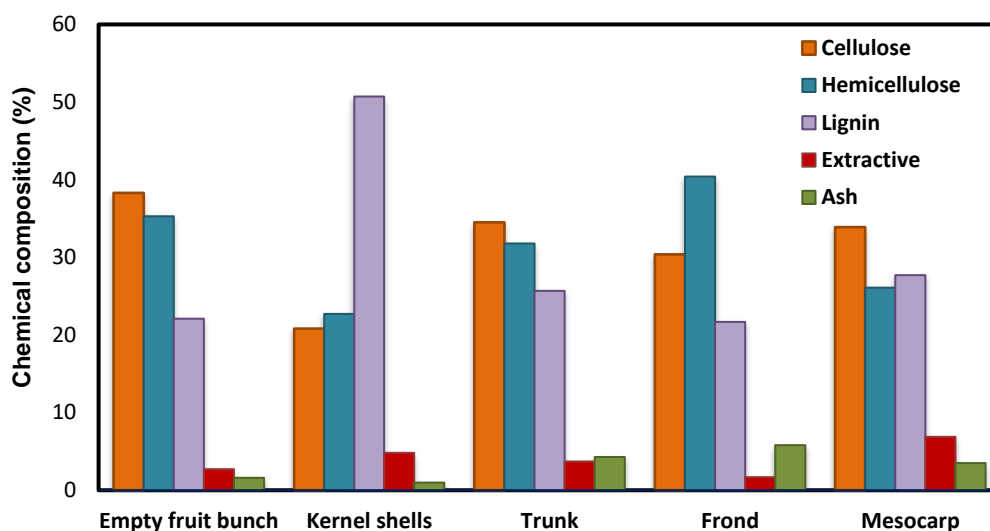


Figure 2.4 Chemical composition of oil palm biomass (Kelly-Yong et al., 2007)

Some articles have reported on utilization of cellulose from empty fruit bunch, for instances cellulose phosphate (Wanrosli et al., 2011; Wanrosli et al., 2013), microcrystalline cellulose (Mohamad Haafiz et al., 2013), cellulose acetate (Djuned et al., 2014; Wan Daud & Djuned, 2015), and nanocrystalline cellulose (Al-Dulaimi & Wanrosli, 2016; Rohaizu & Wanrosli, 2017). It shows that EFB could compete with other plant biomass to produce cellulose or its derivatives at competitive price (Wirjosentono et al., 2004).

2.2 Cellulose Molecular Structure

Cellulose is a linear homopolysaccharide made up of β -1,4 linked anhydro D-glucose units, with polymer chains inter and intra connected by hydrogen bonds. The chemical structure unit of cellulose is basically a repeated segment of cellobiose as shown in Figure 2.5. Cellobiose is a dimer of anhydroglucose unit (AGU) bearing three hydroxyl groups. Obviously, these hydroxyl groups and their ability to form hydrogen bonds play an important role in directing the arrangement of crystalline

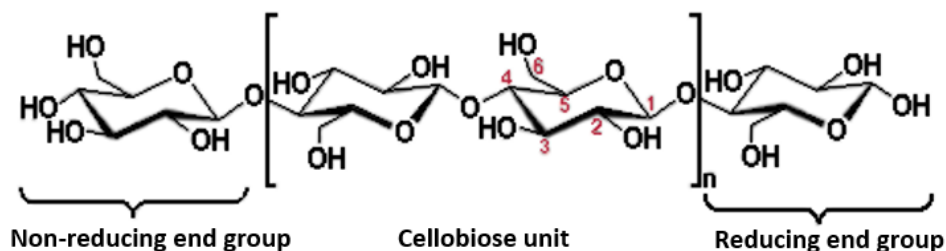


Figure 2.5 Structure of cellulose (Qiu & Hu, 2013)

structure and also generating the physical properties of cellulose (Brinchi et al., 2013; John & Thomas, 2008). Cellulose can exhibit degree of polymerization as much as 10,000 AGU (Klemm et al., 2007).

The unique molecular structure of cellulose leads to its inherent characteristics including hydrophilicity, chirality, degradability, and wide range of chemical variability stimulated by reactivity of the high donor of the hydroxyl groups. Individual cellulose fibers are extremely hydrophilic due to the presence of high amount of hydroxyl groups. It is also the basis for widespread hydrogen bond networks that provide cellulose a massive amount of partially crystalline fiber structure and morphologies (Klemm et al., 2005).

2.2.1 Supramolecular Structure of Cellulose

The properties of cellulose also depend on a defined hierarchical order in structure and organization of its supramolecular, i.e. the chemical system comprising several cellulosic chains known as cellulosic microfibril. The β -1,4 glycosidic linkage allows an intense intra-molecular hydrogen bonding among the groups around the glycosidic bonds, and enables the polymeric chains to be packed side-by-side through inter-molecular hydrogen bonding (Klemm et al., 2005). Subsequently, a planar sheet

consisted of cellulosic chains is generated (Figure 2.9). This supramolecular structure forms the crystalline region of the cellulosic microfibrils. In the same microfibril, however, both crystalline and amorphous regions exist.

The polymorphs of cellulose can be classified into four types; cellulose I, II, III, and IV. Cellulose I, well-known as native cellulose is the most crystalline type that is naturally produced from various organisms. Cellulose I is thermodynamically metastable and can be converted to either cellulose II or III. To date cellulose II has been the most stable of technical significance due to it always produced by Cellulose I and cannot vice versa. It can be prepared via two processes: regeneration (solubilisation and recrystallization) and mercerization (caustic alkali treatments) (Aulin et al., 2010; Šauperl et al., 2009; Siqueira et al., 2010). Cellulose III_I and Cellulose III_{II} are yielded through ammonia treatment of cellulose I or cellulose II, respectively (Klemm et al., 2005). Cellulose IV_I and cellulose IV_{II} are obtained from corresponding form of cellulose III by subsequent thermal treatment in glycerol (Moon et al., 2011). The pathways to yield cellulose II, III, and IV are shown in Figure 2.6.

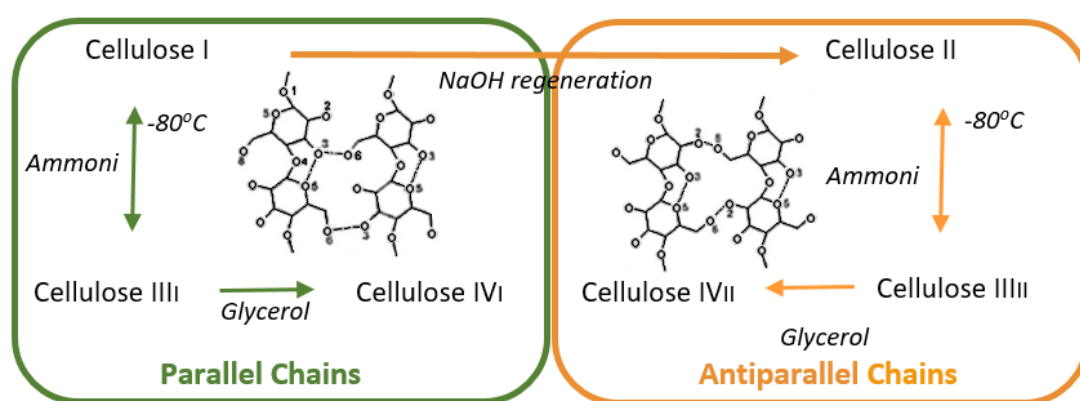


Figure 2.6 Main steps to produce polymorphs of cellulose (Lavoine et al., 2012)

Cellulose I comprise two crystal forms: I_α and I_β . Both can be found in native cellulose structure but their ratio relates to the origins of cellulose. Figure 2.7 illustrates that cellulose I_α crystal is a triclinic unit cell with one cellulose chain, while cellulose I_β is described as a monoclinic unit cell that contains two cellulose chains in a parallel orientation (Moon et al., 2011). The hydrogen bond run in the **a** direction has medium strength (15 kcal mol^{-1}). In the **c** direction, the arrangement is formed by weak van der Waals forces (8 kcal mol^{-1}) and the **b** direction has covalent bond which has the highest strength (50 kcal mol^{-1}).

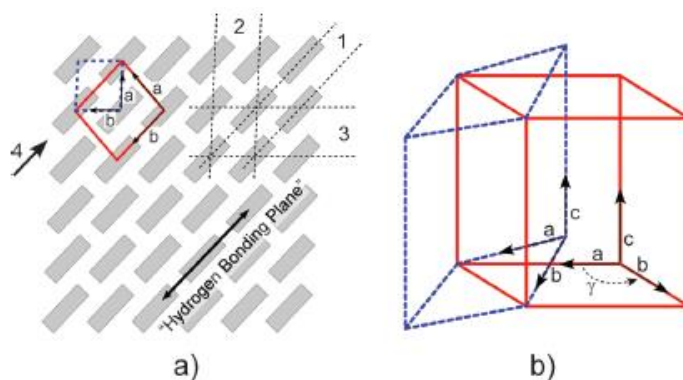


Figure 2.7 Schematic of the unit cells for cellulose I_α (triclinic, dashed line) and I_β (monoclinic, solid line) (Credou & Berthelot, 2014)

In spite of the differences between I_α and I_β unit cell parameters, there are only small shifts chain arrangement in cellulose based on the axis side view. There are three lattice plane labelled 1, 2 and 3 (Figure 2.7), with d-spacing approximately of 0.39 nm, 0.53 nm, and 0.61 nm that are shared and related to I_α lattice plane (110)t, (010)t, and (100)t and for I_β lattice plane (200)m, (110)m and (1T0)m, respectively. The subscripts m and t correspond to monoclinic and triclinic, respectively. However, the notable differences between I_α and I_β is the relative shifting of cellulose sheet (paralleled stacking of cellulose chain in one plane) along the (110)t and (200)m planes in axis direction of the chain (Moon et al., 2011).

In cellulose I, all cellulose chain molecules lay in the same direction from non-reducing to reducing end as illustrated in Figure 2.8. During the mercerization process of native cellulose I with sodium hydroxide, the whole fibers are transformed into a swollen phase, thus the assembly and orientation of microfibrils are totally disturbed. As the result, cellulose II has anti-parallel packing direction (Aulin et al., 2010). The cellulose II has at least three or four anhydroglucose moieties to make the bend. Cellulose II is chemically more reactive than cellulose I. Rayon and cellophane are the example products of cellulose II, regarded as one the most valuable fibers with a wide range applications in chemical industry (Liu & Hu, 2008).

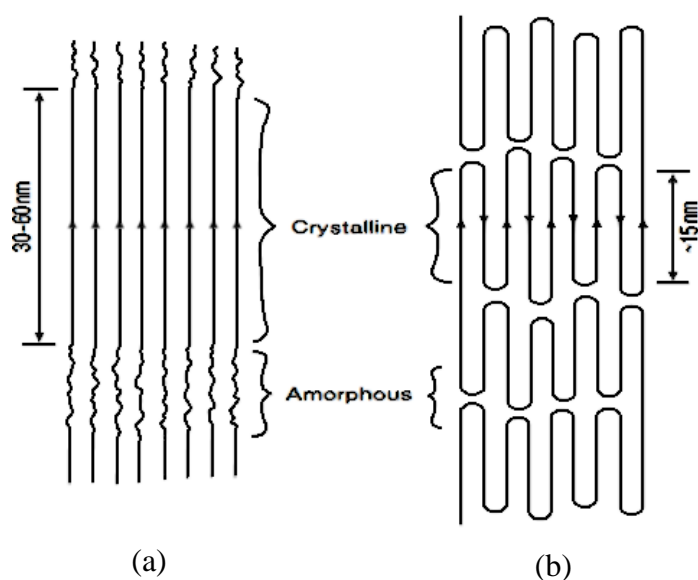
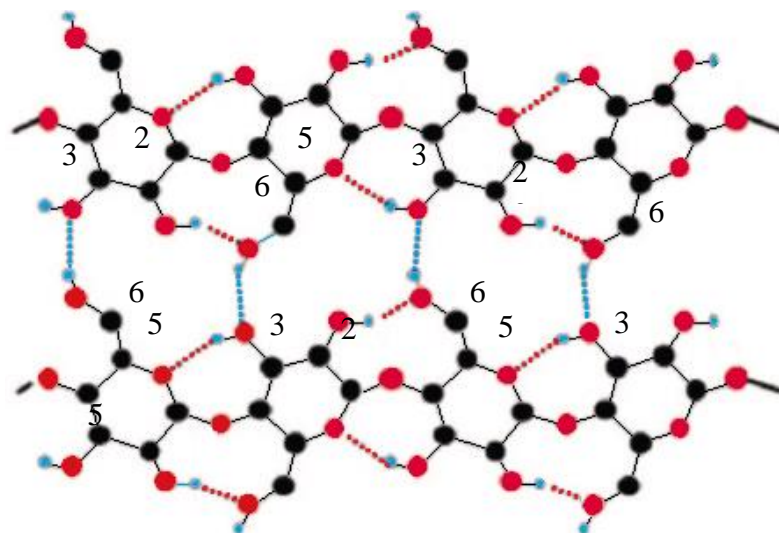
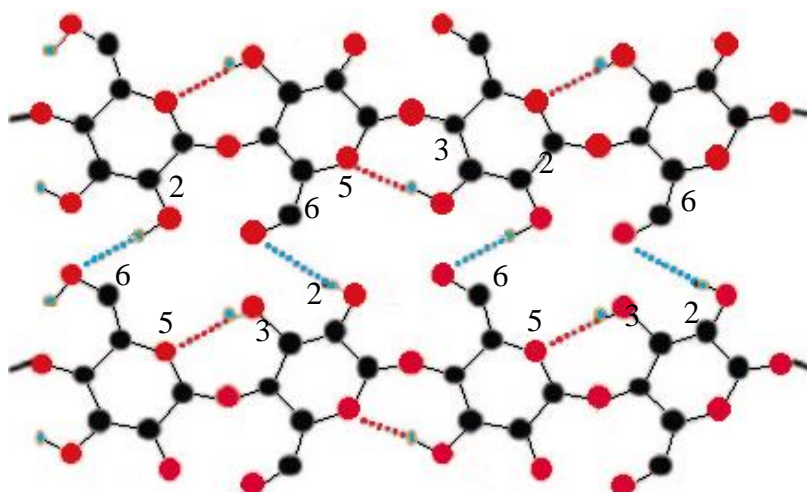


Figure 2.8 Molecule chain direction of (a) cellulose I parallel and (b) cellulose II anti-parallel structure (Macrae et al., 1993)

Cellulose I and cellulose II also differ regarding to the layout of their atoms as shown in Figure 2.9. The main intramolecular O3H–O5' hydrogen bonding is found in both polymorph types. However, the intramolecular O2H–O6' hydrogen bond only exists in cellulose I (both I α and I β). Moreover, intermolecular of cellulose I occurs in O6H–O3'' hydrogen bonds whereas cellulose II forms intermolecular bond via O6H–O2'' and has only one intramolecular O3H–O5' hydrogen bond.



(a) Cellulose I



(b) Cellulose II

Figure 2.9 Supramolecular distinction between (a) cellulose I and (b) cellulose II lies in inter and intramolecular hydrogen bonds (Habibi et al., 2010)

Figure 2.10 shows schematic illustration of cellulose fiber. The intermolecular hydrogen bonds in the crystalline region are strong, consequently the resultant fiber also strong and insoluble in most solvent. The crystalline region also prevents the cellulose from melting. However, in the amorphous region, there are lesser and looser intermolecular hydrogen bonds, to allow forming the hydrogen bond with other molecule for example with water. This generates hygroscopic and hydrophilic features

of the cellulose macromolecule, hence the cellulose swells in water but does not dissolve (Credou & Berthelot, 2014). The amorphous region is more permeable than crystalline regions, enabling water penetration and promoting the enzymatic or acid hydrolysis. During the cellulose purification, the amorphous regions are selectively hydrolyzed and the crystalline parts are released.

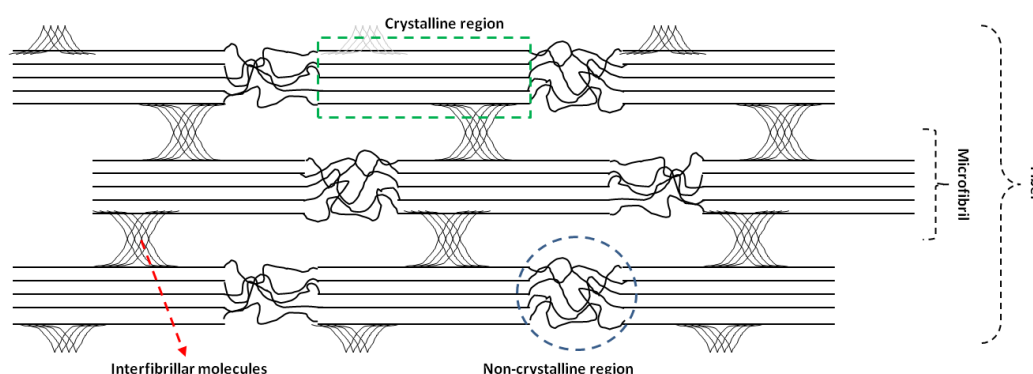


Figure 2.10 Schematics illustration of cellulose microfibril showing one of the suggested configurations of the crystalline and amorphous regions

2.2.2 Morphological Structure

Typical cellulose morphology is organized in a well hierarchical architecture of fibrillary elements, composed of elementary fibrils, microfibrils, and microfibrillar bands as shown in Figure 2.11. The elementary fibril of native cellulose is the smallest morphological unit with about 1.5-3.5 nm diameter whereas the microfibrils has diameter ranging from 10 to 30 nm and the lateral dimension of microfibrillar bands is on the order of 100 nm (Klemm et al., 2011). During the biosynthesis of cellulose, the microfibrils are produced with lengths in several micrometres. Each microfibril has long flexible cellulose chain with cellulose crystal connected along the microfibril axis by disordered amorphous regions (Azizi Samir et al., 2005). Meanwhile, the ordered crystalline region are the packages of cellulose chain that are stabilized by

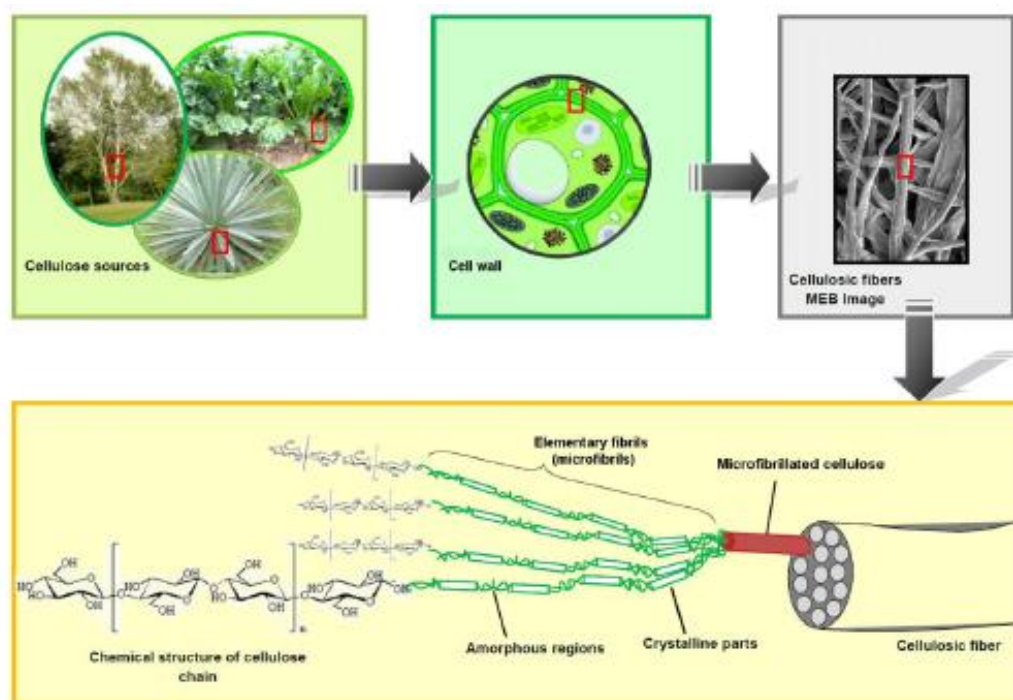


Figure 2.11 From the cellulose source to the cellulose molecules: detail of the cellulosic fiber structure with emphasis on the cellulose microfibrils (Lavoine et al., 2012)

a strong and complex of hydrogen bonds network (explained in Subchapter 2.2.1) that correspond to nanocrystalline rods (Lavoine et al., 2012). Consequently, morphology of the cellulose strongly determines its reactivity. Strong intermolecular hydrogen bonding with close package makes the crystalline region can be completely inaccessible for solvent and reactant, whereas amorphous region is more permeable and the hydroxyl groups accessible to react easily (Sjöström, 1993). Notably, the degree of crystallinity of cellulose and the dimensions of the crystallites vary depending on the sources of cellulose.

The microfibrillar comprised of crystalline phase which has highly ordered region and amorphous phase which alternate with disordered domain. The crystalline phase of fibrils is enclosed or fringed by a very thin layer of paracrystalline (Ioelovich et al., 2010). These elementary forms of cellulose are embedded in a matrix together with hemicelluloses and lignin. The fringes are intermingled with tightly adsorbed

hemicellulose, except cotton which the fibrils contain only cellulose. Meanwhile, lignin is located predominantly on the outer side of microfibril, which is covalently linked to the hemicellulose (Chen, 2014).

2.3 Nanocrystalline Cellulose

Nano size cellulosic particles attract much interest not only because of their supreme typical chemical and physical properties, but also because of their renewability, sustainability, and abundance. Some researchers have reported a widely prospective area of the nanocellulose application, one of those as reinforcing agents in bionanocomposites because of their low cost, light weight, nanoscale dimension, and unique morphology (Habibi et al., 2010; Qiu & Hu, 2013). In general, nanocellulose refers to at least one dimension in nanometer size and can be produced by different method from various lignocellulosic sources (Brinchi et al., 2013). Various terms have been used regarding nano-sized cellulose in literature. Depending on their preparation techniques, the nano-sized cellulosic particles can be classified into two main groups: (1) cellulose nanofibril (CNF) or nano-fibrillated cellulose (NFC), and (2) cellulose nanocrystal (CNC) (TAPPI, 2011). The later also includes the terms of cellulose nanowhisker (CNW) and nanocrystalline cellulose (NCC).

Nanocrystalline cellulose (NCC) is rod-like particles within the range 5-70 nm width and 100 to several micrometer lengths. Its morphological dimension is characterized in axial ratio that is defined as the ratio of length to diameter. Higher NCC axial ratio gives larger specific surface area and may contribute to better mechanical and thermal properties of bionanocomposites (Kargarzadeh et al., 2012). NCC is a pure (100%) cellulose with degree of crystallinity in the range of 54-88% (Moon et al., 2011). The dimension, degree of crystallinity, and morphologies depend

on the cellulose source and condition of preparation is carried (Habibi et al., 2010; Sacui et al., 2014).

The different types of nano-sized cellulose exhibit distinct properties which decide their functionality and applicability, meaning that certain types of nano-sized cellulose, suitable for specific application than others. The properties of nanocellulose are unique including high Young's modulus (approximately 150 GPa), tensile strength (around 10 GPa), low density (around 1.566 g.cm⁻³), large surface area (about several hundred of m².g⁻¹), a highly crystalline nature, a wide range of axial ratios can be accessed, and potential compatibility with other materials such as protein, polymer, and living cells (Dufresne, 2012; Dufresne et al., 2003; Silv rio et al., 2013). Moreover, the options for material and chemical processing of nanocellulose are exceptionally flexible, creating a wide range of opportunities in terms of structure and functionality (Abitbol et al., 2016). This uniqueness makes the NCC as a potential reinforcement material to improve strength, stiffness, and toughness through its interaction with the matrix in composites.

With the latest progress on conversion and separation technologies, the hierarchical structure of biomass can be broken-down and incorporated into bio-based nanoproducts. Various systematic methods had been reported to synthesize nano-sized cellulose, i.e. chemical, biological fermentation, mechanical, physical, or a combined process. Table 2.2 shows different nano-sized cellulose derived by various approaches. According to Kopania et al. (2012), the first report of microfibril isolation date back to 1983 (Herrick et al., 1983; Turbak et al., 1983) with starting material being wood cellulose (softwood). Later, non-wood material is also investigated as source of cellulose, including isolation of nanofibers from wheat straw and soybean hulls

Table 2.2 The difference between TEMPO-oxidized NNC, MFC, and CNC/CNW

Type of nanocellulose	TEMPO-oxidized NNC	MFC	CNC or CNW
Preparation Method	TEMPO-mediated oxidation of wood cellulose, and mild disintegrated of oxidized cellulose in water	Repeated high-pressure homogenizer treatment of wood cellulose/water slurry	Acid hydrolysis of wood cellulose with 64% H ₂ SO ₄ and disintegration of the residue in water
Yield	>90%	≈100%	<50%
Morphology	Uniform width of 3-4 nm, <2-3 μm in length	Uneven width of 10-2000 nm forming bundles	Uneven width 5-10 nm, <300 nm in length, spindle like whiskers, forming partial bundle
Energy consumption in nano conversion	< 7 MJ/kg	700-1400 MJ/kg	< 7 MJ/kg

Source: (Isogai et al., 2011)

(Alemdar & Sain, 2008) impact of the lignification of bamboo nanofibers (Okahisa et al., 2011), banana nanofibers using steam explosion process (Deepa et al., 2011), and nanowhiskers from bagasse (Teixeira et al., 2011).

2.3.1 Acid Hydrolysis

The most well-known method to isolate nano-sized cellulose from cellulose fibers is acid hydrolysis (Azzam et al., 2010; Frone et al., 2016; Robles et al., 2015; Zoppe et al., 2010). The schematic illustration for the isolation of the crystalline part of cellulose through acid hydrolysis is presented in Figure 2.12. The acid hydrolysis involves the attacking of non-crystalline cellulose polymer chain hydrolytically, to cleave the glycosidic linkage between cellobiose units. Amorphous or paracrystalline

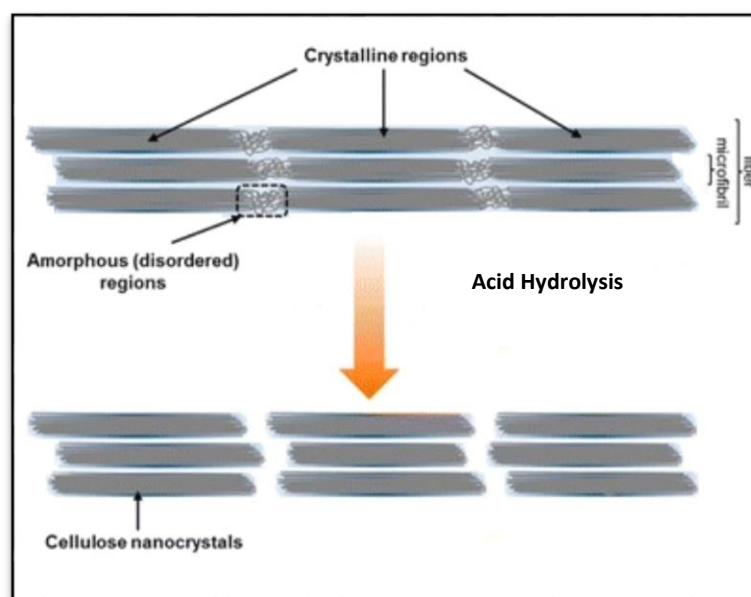


Figure 2.12 Schematic illustration for the isolation of the crystalline structure of cellulose by acid hydrolysis (Mohan et al., 2015)

domains of cellulose are selectively hydrolyzed by sulfuric acid or hydrochloric acid, while crystalline domain which is relatively inaccessible remains intact even though attacked by strong acid. Longer hydrolysis time induces a fast reduction in degree of polymerization through cleavage of the accessible amorphous domain of the long axis cellulose thus decrease in nanocrystal length. However, the crystalline region could be then partially destroyed when the treatment involves a high concentration of acid and prolonged time.

During the hydrolysis with sulfuric acid, the intramolecular and intermolecular hydrogen bonds are weakened and split leading to the formation of sulphate on the surface of cellulose complex. The presence of negative charge on the surface of nanocellulose will lead to anionic stabilization, where repulsion forces of electrical double layers avoid nanocellulose particles to agglomerate (Ioelovich, 2012; Satyamurthy & Vigneshwaran, 2013). In addition, mechanical effect such as sonication occasionally is used to boost the breakdown of cellulose structure into nano-

sized crystalline (Abraham et al., 2011). Then, rod-like nanocrystals are produced in aqueous solution (Habibi et al., 2010; Qiu & Hu, 2013). Acid hydrolysis, however, has relatively low yield at only 30–50% (Börjesson & Westman, 2015; Isogai et al., 2011). In addition, the hydrolysis using sulfuric acid causes significant reduction in thermal stability of the cellulose.

2.3.2 TEMPO-Oxidation of Cellulose

TEMPO (2,2,6,6-tetramethylpiperidine-1-oxyl radical) oxidation has become an alternative technique to isolate nano-sized cellulose due to some advantages. In principle, TEMPO-mediated oxidation is a method for selectively modifying the native cellulose surface under mild and aqueous environment (Saito & Isogai, 2004; Saito et al., 2006a; Saito et al., 2006b). Such modifications lead to weakening adhesion among cellulose fibrils by preventing the formation of intermolecular hydrogen bonding (Missoum et al., 2013). The basic principle of this treatment is oxidation of cellulosic fibers by NaClO in the presence of TEMPO and NaBr as catalysts in aqueous solution at room temperature and pH of 10-11. The C6 primary hydroxyl groups of cellulose are thus selectively converted to sodium carboxylate groups via the C6 aldehyde groups according to the mechanism shown in Figure 2.13, and only NaClO is consumed (Missoum et al., 2013; Saito et al., 2007). The amount of NaClO in the system influences the carboxylic yielded; the higher amount of NaClO results in the higher carboxylic group on the cellulose surface and the higher reduction in the degree of polymerization. Isogai's group (Saito et al., 2006a; Saito et al., 2006b) applied the TEMPO-mediated oxidation on cellulose from various sources such as wood pulp, tunicate, cotton linters, ramie, and bacterial cellulose. Figure 2.14

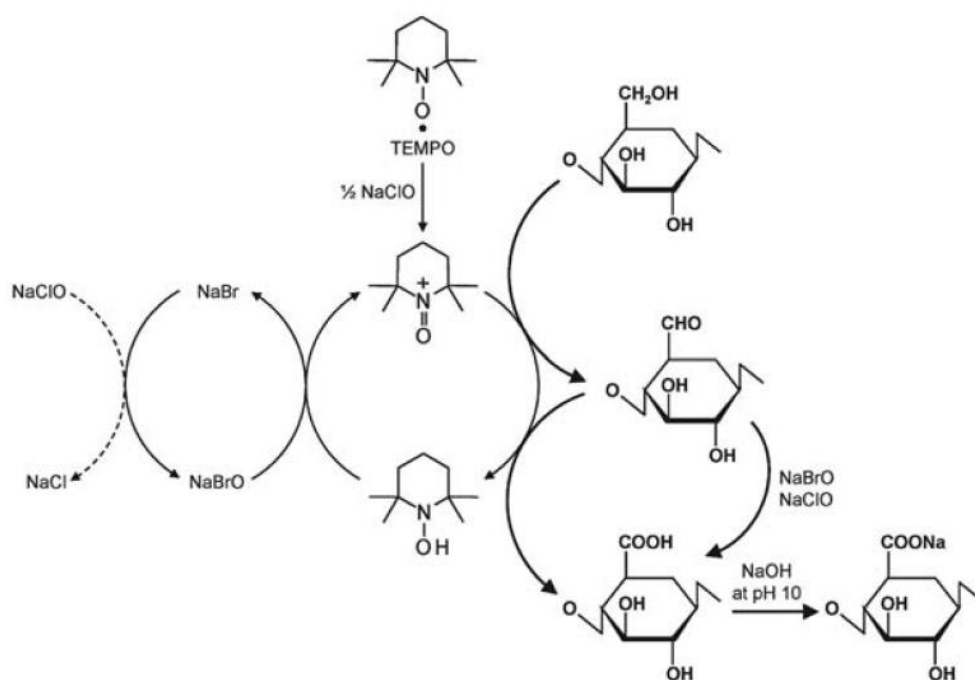


Figure 2.13 Mechanism of regioselective oxidation of cellulose by TEMPO-mediated oxidation (Isogai et al., 2011)

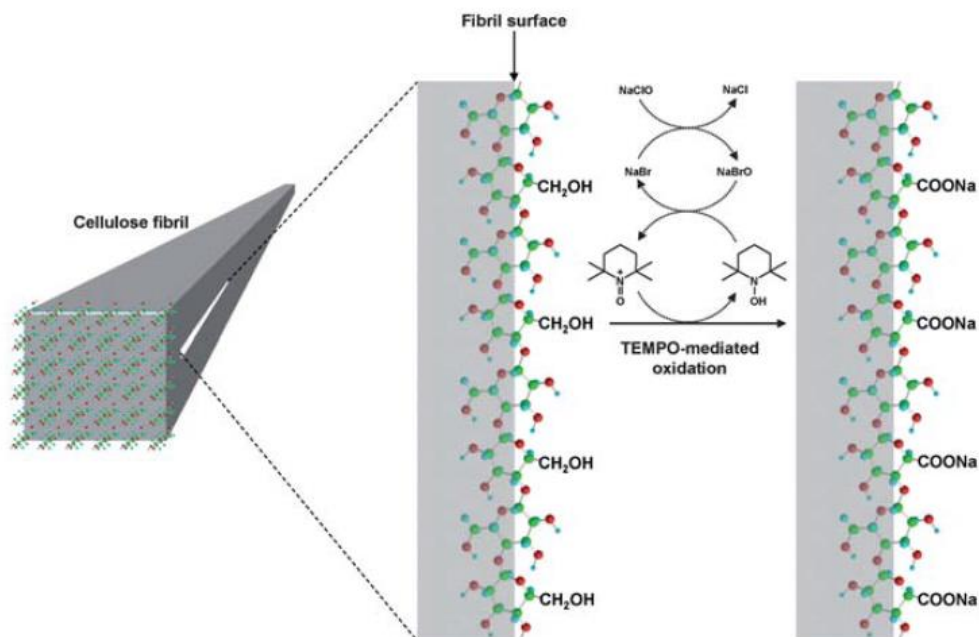


Figure 2.14 Illustration for the oxidation of C6 primary hydroxyls on native cellulose microfibril surfaces to C6 carboxylate groups using the TEMPO system (Isogai et al., 2011)

illustrates considerable amounts of sodium carboxylate groups exist in the TEMPO-oxidized native celluloses, allowing the hydrophilic character, thermal degradation behaviour, and other properties of TEMPO oxidized celluloses can be tailored to some extent by various methyl esterification, metal-ion exchange, and other possible chemical modification of the carboxylate groups (Fukuzumi et al., 2010; Zhang et al., 2006). The TEMPO-mediated oxidation of native cellulose demonstrates that although the oxidation take place at entire part of the fibers, but only the accessible primary hydroxyl group could be transformed, mostly on the outer side of the microfibrils by the reaction with carboxylate anion groups (Eichhorn et al., 2010; Saito et al., 2006a).

Compared to energy usage by the fully mechanical disintegration method in high pressure homogenizer (700–1400 MJ/kg) in, treatment of cellulose by TEMPO-mediated oxidation significantly reduces the energy consumption to less than 7 MJ/kg. The nanofibrils of the cellulose fibers can separate from each other readily due to repulsive forces of the carboxylate anion groups (Eichhorn et al., 2010; Missoum et al., 2013). Furthermore, the TEMPO oxidized nanofibrils within the fibres is readily disintegrated by mechanical treatment such as sonication or chopper, and concurrently with repulsive forces between ionized carboxylates overcoming the numerous of hydrogen bonds that hold the nanofibrils together. As a result, the nanocellulose in water suspension (3–5 nm diameter) are directly yielded from the TEMPO-mediated oxidized pulp (Eichhorn et al., 2010; Saito et al., 2006a). In addition to the induction of a negatively charged surface, the advantage of TEMPO-mediated oxidation process includes its higher recovery of oxidized nanocellulose of more than 90% on OPEFB